Regular Article

blood

MYELOID NEOPLASIA

Establishing human leukemia xenograft mouse models by implanting human bone marrow–like scaffold-based niches

Antonella Antonelli,[1] Willy A. Noort,[2] Jenny Jaques,[1] Bauke de Boer,[1] Regina de Jong-Korlaar,[2] Annet Z. Brouwers-Vos,[1] Linda Lubbers-Aalders,[2] Jeroen F. van Velzen,[3] Andries C. Bloem,[3] Huipin Yuan,[4] Joost D. de Bruijn,[5] Gert J. Ossenkoppele,[2] Anton C. M. Martens,[2] Edo Vellenga,[1] Richard W. J. Groen,[2] and Jan Jacob Schuringa[1]

[1]Department of Experimental Hematology, Cancer Research Center Groningen, University Medical Center Groningen, University of Groningen, The Netherlands; [2]Department of Hematology, Vrije Universiteit Medical Center, Amsterdam, The Netherlands; [3]Department of Immunology, University Medical Center Utrecht, Utrecht, The Netherlands; [4]Xpand Biotechnology BV, Bilthoven, The Netherlands; and [5]Queen Mary University of London, School of Engineering and Materials Science, London, United Kingdom

Key Points

- Humanized niche xenograft mouse models were generated that enabled engraftment of patients' leukemia cells covering all risk groups.
- Self-renewal was better maintained in the humanized niches as determined by serial transplantation and genome-wide transcriptome studies.

To begin to understand the mechanisms that regulate self-renewal, differentiation, and transformation of human hematopoietic stem cells or to evaluate the efficacy of novel treatment modalities, stem cells need to be studied in their own species-specific microenvironment. By implanting ceramic scaffolds coated with human mesenchymal stromal cells into immune-deficient mice, we were able to mimic the human bone marrow niche. Thus, we have established a human leukemia xenograft mouse model in which a large cohort of patient samples successfully engrafted, which covered all of the important genetic and risk subgroups. We found that by providing a humanized environment, stem cell self-renewal properties were better maintained as determined by serial transplantation assays and genome-wide transcriptome studies, and less clonal drift was observed as determined by exome sequencing. The human leukemia xenograft mouse models that we have established here will serve as an excellent resource for future studies aimed at exploring novel therapeutic approaches. (*Blood*. 2016;128(25):2949-2959)

Introduction

Despite a continuous improvement in xenograft models for studying human hematopoiesis in vivo, engraftment of human malignant cells remains challenging. To study the molecular mechanisms involved in human leukemias and to improve treatment options, it is critically important to establish in vivo xenograft models that faithfully recapitulate the disease. Even the most immunodeficient NOD-SCID IL2Rγ$^{-/-}$ (NSG) mouse strains, which are frequently used, have serious drawbacks because in vivo myeloid transformation has been difficult to achieve,[1-5] and a large proportion of primary acute myeloid leukemia (AML) samples fail to engraft, in particular those that belong to the prognostically favorable subgroups.[6-8] These observations suggest that a specific human microenvironment might be necessary to faithfully recapitulate human myeloid leukemias in vivo in xenograft models.

Because certain myeloid growth factors are often species-specific, the murine bone marrow (BM) niche is most likely not sufficient for providing the appropriate environment for human leukemic stem cells. NOD/SCID-3/GM/SF mice engineered to produce human interleukin-3 (IL-3), granulocyte-macrophage colony-stimulating factor (GM-CSF), and steel factor/stem cell factor,[9-11] and NSG mice expressing human IL-3, GM-CSF, and stem cell factor (NSG-SGM3)[8] have been generated, and enhanced engraftability of primary human AML samples was observed in these mouse strains. In addition, the expression of these 3 human growth factors was sufficient to allow AML development upon transplantation of cord blood CD34$^+$ cells expressing MLL-AF9.[8] Various other mouse strains have also been developed,[11-17] including MISTRG mice expressing macrophage colony-stimulating factor, IL-3, GM-CSF, thrombopoietin, and signal regulatory protein α,[12] and are therefore useful tools, although other human niche-specific factors might still be missing.

Here, we made use of a humanized niche xenograft model in which ceramic scaffolds coated with human mesenchymal stromal cells (MSCs) were implanted in immunodeficient mice.[18,19] This resulted in the creation of a humanized niche in which MSCs developed into bone, adipocytes, and various other stromal components. A large cohort of primary AML patients provided samples that covered all of the important genetic and risk subgroups, and those samples were transplanted into the humanized niche xenograft models. Our data indicate that the presence of a humanized microenvironment favors

Submitted 26 May 2016; accepted 25 September 2016. Prepublished online as *Blood* First Edition paper, 12 October 2016; DOI 10.1182/blood-2016-05-719021.

The online version of this article contains a data supplement.

There is an Inside *Blood* Commentary on this article in this issue.

The publication costs of this article were defrayed in part by page charge payment. Therefore, and solely to indicate this fact, this article is hereby marked "advertisement" in accordance with 18 USC section 1734.

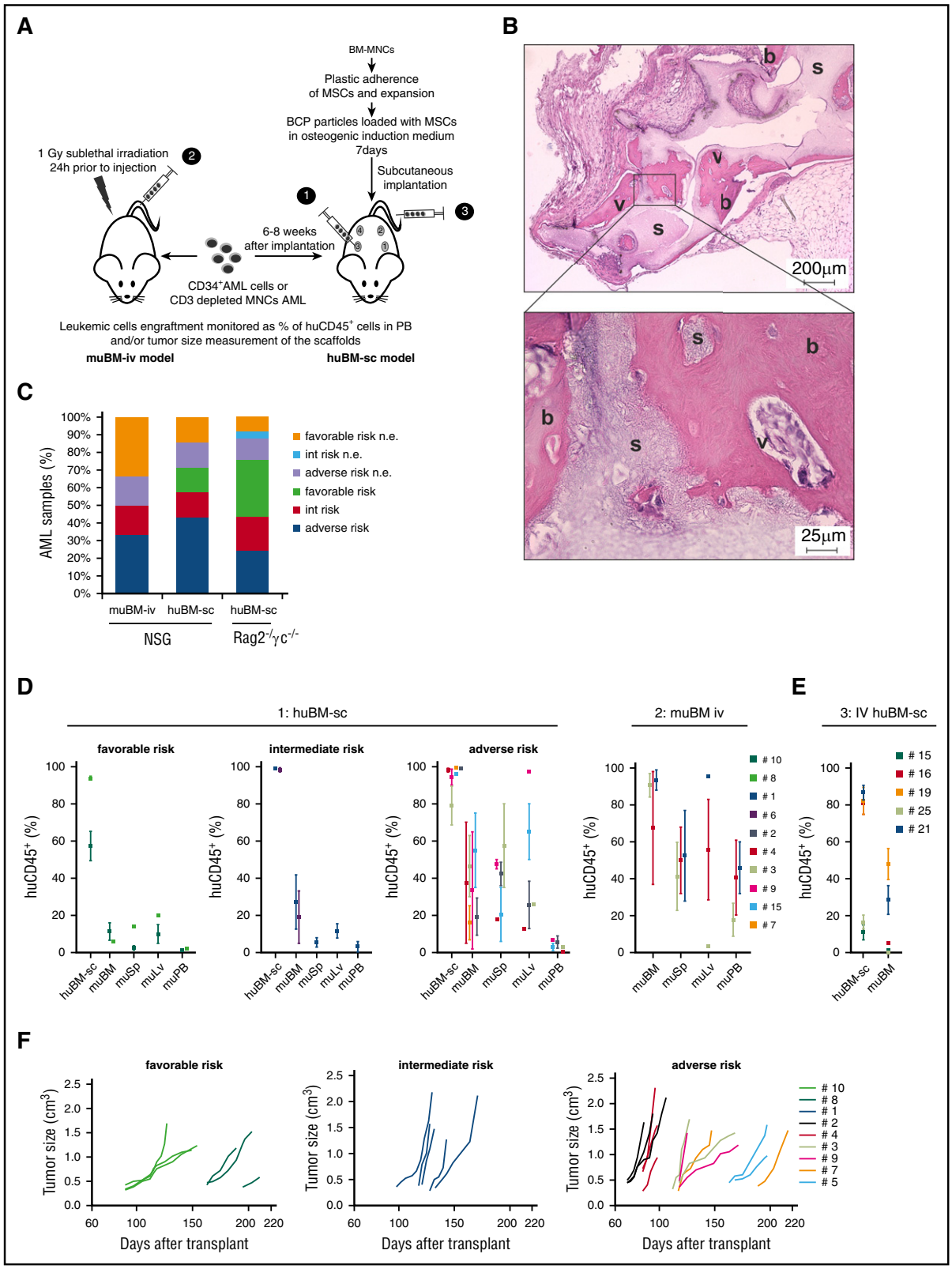

Figure 1. Overview of the mouse xenograft leukemia models. (A) Schematic representation of the generation of muBM-iv and huBM-sc models. (B) Representative hematoxylin and eosin (H&E) stain of scaffold sections 6 weeks after implantation. b, bone; s, scaffold; v, blood vessels. (C) Success rate of leukemia development in muBM-iv and huBM-sc models, expressed as percentage of AML samples from different risk groups, which engrafted or not in the 2 xenograft models. (D) Scatter plots showing engraftment of donor human CD45$^+$ cells in different compartments of the mouse at euthanasia. Engraftment values from several mice for each AML sample are expressed as mean ± standard error of the mean (SEM). Route 1: cells were directly injected into the humanized scaffolds; route 2: cells were injected intravenously into mice without humanized scaffolds. (E) Experiment as in (D), but now cells were injected intravenously into mice carrying humanized scaffolds. (F) In vivo tumor growth rates of the biggest tumor scaffold in each mouse. Each colored line represents 1 mouse from a certain AML sample. Tumor size (cm^3) was used as the end point of the experimental period. int, intermediate; muSp, murine spleen; muLv, murine liver; muPB, murine peripheral blood; n.e., no engraftment.

engraftment of AML patient samples, including favorable-risk AML samples that are notoriously difficult to engraft in NSG mouse strains and that self-renewal is better maintained in the human niche.

Methods

Establishment of the humanized scaffold niche xenograft model and transplantations

The ectopic bone model was established as described previously.[18,19] Briefly, 4 to 6 hybrid scaffolds consisting of three 2- to 3-mm biphasic calcium phosphate particles loaded with human MSCs were implanted subcutaneously into female NOD.Cγ-Prkdc^{scid} Il2rγ^{tm1Wjl}/SzJ (NSG) or RAG2$^{-/-}$γc$^{-/-}$ mice. Eight weeks after scaffold implantation, different cell doses ranging from 5×10^4 to 4×10^6 were directly injected into the scaffolds as indicated during primary and secondary transplantations.

Patient samples

Peripheral blood (PB) and BM from untreated patients diagnosed with AML, blast-crisis chronic myeloid leukemia, or B-cell acute lymphoblastic leukemia at the University Medical Center Groningen (UMCG) or Vrije Universiteit Medical Center (VUMC) were studied after patients provided informed consent and the protocol was approved by the Medical Ethical Committee of the UMCG or VUMC, in accordance with the Declaration of Helsinki. After Ficoll separation of mononuclear cells (MNCs), cells were cryopreserved until further use. CD34$^+$ cells were enriched or CD3$^+$ cells were depleted by using a magnetically activated cell-sorting CD34 progenitor kit or automatically by using an autoMACS separator (Miltenyi Biotech) as described previously.[3,20] Additional methods are described in the supplemental Data, available on the *Blood* Web site.

Results

Establishing xenograft human leukemia models that use three-dimensional scaffolds coated with human MSCs

A cohort of 39 patients was selected for establishing humanized niche mouse xenograft leukemia models (17 [44%] of 39, adverse-risk group; 8 [21%] of 39, intermediate-risk group; and 14 [36%] of 39, favorable-risk group; supplemental Table 1). Cells were injected into a humanized model that was based on subcutaneous implantation of human BM–like scaffolds (huBM-sc) to provide a human microenvironment, as described previously.[18,19] Briefly, in this model, ceramic scaffolds coated with human MSCs were implanted subcutaneously in immunodeficient mice where they developed into structures mimicking a human BM microenvironment, including bone formation, and ossicles were vascularized by murine blood vessels (Figure 1B; supplemental Figure 1,2A). Six to 8 weeks later, CD34$^+$- or CD3$^+$-depleted AML MNCs were then injected into these so-formed ossicles. As a comparator, 6 of the patient samples were also injected intravenously into mice (referred to as muBM-iv) without human scaffolds to evaluate engraftment in a murine microenvironment (Figure 1A; supplemental Table 1). As a second comparator, cells were injected either directly into the scaffold or intravenously into mice that carried humanized scaffolds in 5 selected cases (referred to as IV huBM-sc; Figure 1A,E). Experiments were carried out independently in 2 institutes using 2 different mouse strains: NSG (at the UMCG in The Netherlands) and Rag2$^{-/-}$γc$^{-/-}$ mice (at the VUMC in The Netherlands) (supplemental Table 1) showing robustness of the model. Leukemic cell engraftment was monitored over time with PB sampling and/or by monitoring tumor volume in the scaffolds (Figure 1A; supplemental Table 2). Hematoxylin and eosin staining of noninjected scaffold sections 6 weeks after implantation confirmed the presence of extramedullary bone in the scaffolds. Different magnifications revealed the presence of stromal cells and bone material deposited in the cavities of the ceramic particle, and blood vessels of mouse origin were also observed (Figure 1B; supplemental Figure 1A,2A).

For huBM-sc mice, chimerism levels in the PB were usually low (supplemental Table 2), so the volume of the biggest tumor growing on 1 of the scaffolds at approximately 1.5 to 2 cm^3 was defined as the end point of the experiment. muBM-iv mice were euthanized when we observed huCD45$^+$ levels in the PB of ~30% to 60% of total living cells along with signs of illness. We obtained engraftment and outgrowth of leukemic cells in 3 (43%) of 7 cases with the muBM-iv model and in 29 (74%) of 39 cases in the huBM-sc model. Lack of engraftment was not the result of an absence of bone formation in the scaffolds (supplemental Figure 1B). Notably, favorable-risk leukemias engrafted only in the huBM-sc model, but no engraftment was observed in any of the muBM-iv mice without humanized scaffolds, and the same was true for patient sample #2, which also did not engraft in the muBM-iv model (Figure 1C; supplemental Table 1). All 7 favorable-risk AMLs with an inv16, which are notoriously difficult to engraft in NSG mice, efficiently engrafted in the huBM-sc mice (supplemental Table 1). AML #1 engrafted in both the huBM-sc and the muBM-iv models with similar kinetics of leukemia development, whereas AMLs #3 and #4 engrafted in the muBM-iv model but with slower kinetics compared with the huBM-sc model (supplemental Table 2).

All intermediate-risk samples engrafted in both models (Figure 1C-D). Interestingly, in huBM-sc mice, leukemic cells engrafted in the humanized scaffold niches and also seeded into murine hematopoietic organs, with engraftment levels in murine compartments increasing concomitantly with prognosis of disease (eg, the percentage of human leukocytes in murine BM ranged from 4% to 20% in the favorable-risk mice whereas chimerism levels in murine BM, spleen, and liver were significantly higher in mice injected with adverse-risk samples reaching an average of 55% in one case of adverse-risk leukemia (Figure 1D). Five AML samples were injected intravenously in mice that carried humanized scaffolds (Figure 1A, route 3). All samples efficiently seeded into the scaffolds whereas in only 2 of 5 cases engraftment was observed in the human BM (Figure 1E).

The onset of tumor initiation and consequently the time of euthanasia (14 to 38 weeks) were variable from patient to patient, with tumor growth rates that seemed to correlate with risk group. In the majority of animals, tumors were palpable 100 days after injection with the exception of 2 cases of adverse-risk AML (#2 and #4) in which the onset was earlier than 100 days (Figure 1F; supplemental Table 2). Furthermore, by using a luciferase gene–marked AML sample, we observed that growth was initiated 50 days after engraftment (supplemental Figure 2C). In all cases of engrafted intermediate- and adverse-risk leukemias, the growth rate (read out by the slope of the curve) was faster than in favorable-risk AMLs (Figure 1F; supplemental Table 2).

Leukemic cells engrafted in huBM-sc mouse models recapitulate the original phenotype of the patient

The immunophenotype of the leukemic cells of the original patient samples was compared with that of tumor cells isolated from the human scaffold niche and from the murine compartments by using fluorescence-activated cell sorting. In some cases, the original patient immunophenotype was well conserved in vivo regardless of whether the cells expanded in a humanized or murine

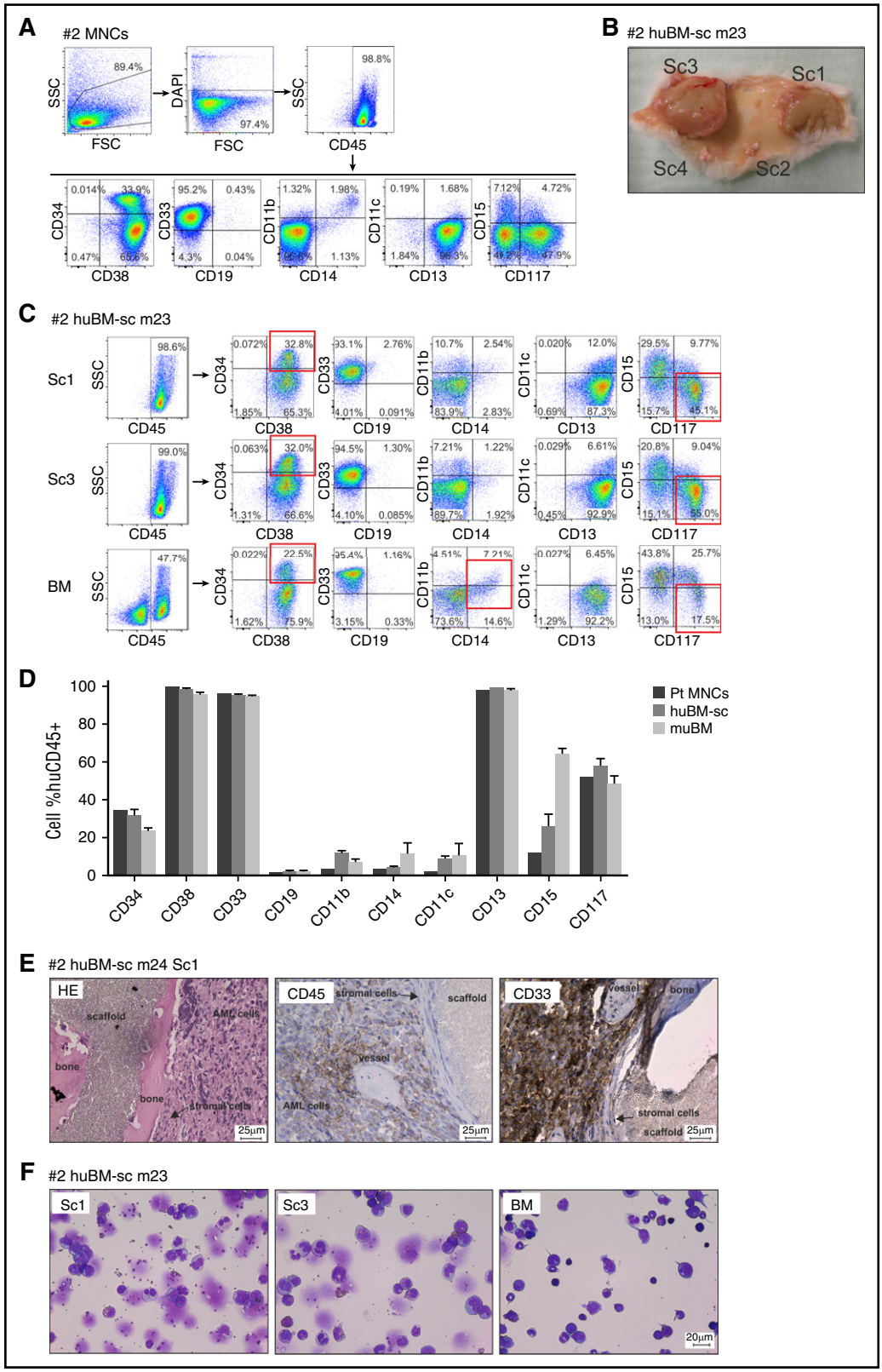

Figure 2. Mouse xenograft AML model using sample AML #2. (A) Fluorescence-activated cell sorting (FACS) immunophenotype of AML #2 patient-derived MNCs. (B) Representative photograph depicting the leukemic masses formed around the extramedullary bones of scaffold 1 (Sc1) and Sc3 and 2 scaffolds with no tumor growth (Sc4, not injected control scaffold), at mouse euthanasia. (C) Representative FACS phenotype from a primary huBM-sc mouse (m23; supplemental Table 1) transplanted with AML #2 cells. Expression of a panel of hematopoietic markers in huCD45^{+} gated cells isolated from different scaffolds or from the murine BM. (D) Bar graph summarizing the FACS phenotype of human CD45^{+} cells from different compartments of all mice injected with #2 AML cells compared with the original patient phenotype. Values are expressed as mean ± SEM. (E) Histologic sections of scaffold tumor from a representative #2 huBM-sc mouse (m24, Sc1) stained with H&E, anti-huCD45, or anti-huCD33 antibodies. (F) Representative images (m23) of May-Grünwald-Giemsa–stained cytospins of cells retrieved from Sc1, Sc3, or BM. DAPI, 4′,6-diamidino-2-phenylindole; FSC, forward scatter; pt, patient; SSC, side scatter.

microenvironment, whereas in other cases, the original patient immunophenotype was clearly better preserved in the humanized scaffolds. An example of the latter is AML #2. This sample contained an inv16 and a t(9;22) BCR-ABL translocation with no mutations in NPM or FLT3. At presentation, this patient displayed a relatively large immature population of blast cells (34% $CD34^+$ and 48% $CD117^+CD15^-$), and all MNCs were positive for CD33 and CD13, weakly positive for CD14, CD11b, CD11c, and CD15, and negative for CD19 (Figure 2A). $CD34^+$ blast cells were isolated from this patient and injected into the scaffolds of NSG mice, and within 14 weeks, tumors developed on the scaffolds and the animals were euthanized (Figure 2B; supplemental Table 2). Scaffold tumors were greenish (indicating the presence of myeloid myeloperoxidase–expressing cells) and were well vascularized with murine blood vessels. Leukemic cells could also be retrieved from murine BM, spleen, liver, and PB (supplemental Table 2). Cells retrieved from the humanized scaffolds were $huCD45^+$ with percentages of $CD34^+$ and $CD117^+$ comparable to those at diagnosis, whereas in cells retrieved from BM, the percentage of $CD34^+$ and especially $CD117^+$ cells was partially reduced, whereas percentages of CD15 and to some extent CD11b and CD14 were increased (Figure 2C-D). Histologic analysis using hematoxylin and eosin staining confirmed that scaffold tumors contained bone and $huCD45^-$ stromal cells surrounded by huCD45 and $huCD33^+$ AML blasts (Figure 2E). May-Grünwald-Giemsa staining of cytospins confirmed that scaffold tumors contained primarily immature blast-like cells with big nuclei, and BM samples revealed a more abundant presence of smaller cells with a more differentiated morphology (Figure 2F).

In the case of AML #1, the humanized niche did not clearly confer an advantage to preserve a more immature phenotype compared with the murine stromal environment (supplemental Figure 3). This sample contained an FLT3 internal tandem duplication (FLT3-ITD), was NPM wild-type (wt), and contained several chromosomal abnormalities including a t(3;5) NPM-MLF1 translocation, with a high percentage of $CD34^+/CD117^+$ blasts (supplemental Figure 3A). Within 100 to 150 days, tumors were visible, and again infiltration of human $CD45^+$ cells was observed in mouse organs (supplemental Figure 3B-C; supplemental Table 2). However, the immunophenotype of the original patient sample #1 was now conserved in the humanized niche as well as in mouse niches (supplemental Figure 3C-F).

Leukemic cells isolated from humanized scaffolds have superior secondary transplantation capacity compared with those isolated from the murine BM niche

Secondary transplantation assays were performed for 3 cases by using various doses ranging from 4.5×10^4 to 3×10^6 cells harvested from scaffolds or BM that were injected into individual scaffolds of secondary mice (Figure 3A). Secondary engraftment transplantation into second scaffolds could readily be established for huBM-sc–harvested cells in all investigated cases (Figure 3A-G; supplemental Figure 2D). For AML #2, secondary transplantation could readily be established for huBM-sc–harvested cells with 3×10^6, 1×10^6, and even 4×10^5 cells, but no secondary engraftment was observed for muBM-iv–harvested cells using up to 4×10^5 cells (Figure 3B-C; supplemental Table 2). The same was true for AML #3, whereby secondary engraftment was observed with 1.5×10^6 and 1×10^5 injected huBM-sc–harvested cells, but not with up to 4×10^5 muBM-iv–harvested cells (Figure 3D-E; supplemental Table 2). For AML #1, secondary engraftment could be established with as little as 4.5×10^4 huBM-sc–harvested cells, which was not seen with muBM-iv–harvested cells when injected at the same dose, but injection of 1.8×10^5 muBM-iv–harvested cells did allow secondary transplantation, albeit with slower kinetics compared with huBM-sc–harvested cells at the same dose (Figure 3F-G; supplemental Table 2). These data seemed to be in line with flow cytometry analyses on stem/progenitor compartments suggesting that the immature $CD34^+/CD38^-$ compartments were better preserved in the human niches (supplemental Figure 4A). Together, these data again point to the notion that stemness was better preserved in the humanized niche for most leukemias, whereby AML #1 seemed to be the least dependent on a human microenvironment within the tested cohort, in line with our observation that this patient sample was also able to engraft in the muBM-iv model, whereas AML #2, for example, seemed to be much more dependent on cues from a human microenvironment. We also analyzed lymphoid engraftment but did not find any $CD3^+/CD4^+$ or $CD3^+/CD8^+$ cells (supplemental Figure 4B).

Next, we compared engraftment of favorable-risk, intermediate-risk, and adverse-risk samples in mice carrying scaffolds coated with either human MSCs or murine MSCs and performed primary and secondary engraftment experiments (Figure 4A). The adverse-risk sample engrafted in both conditions, regardless of whether scaffolds were coated with human or murine MSCs (Figure 4B). The intermediate-risk sample showed the highest chimerism levels in scaffolds coated with human MSCs compared with murine MSCs, and secondary engraftment was observed only with cells harvested from human scaffolds (Figure 4B). Finally, the favorable-risk sample efficiently engrafted in the human scaffolds but only at very late time points in the murine scaffolds (day 322) (Figure 4B). Efficient secondary transplantation was observed in all 3 cases in mice carrying scaffolds coated with human MSCs. No significant differences were seen in secondary transplantation of adverse-risk sample #27 when scaffolds coated with human vs murine MSCs were compared, but significantly delayed secondary engraftment was observed with intermediate-risk sample #18 in the scaffolds coated with murine MSCs. Failure of engraftment in the murine scaffolds was not a result of insufficient formation of an extramedullary murine niche (Figure 4D).

Evaluation of clonal heterogeneity and clonal drift within humanized and murine niches

We selected three cases (#1, #2, and #3) for evaluating clonal heterogeneity and clonal drift. Variant allelic frequencies (VAFs; exome sequencing) of recurrent mutations were determined in patient samples at presentation and in tumor material harvested from the humanized scaffold niche, from the murine BM niche, and from in vitro expanded AML on MS5 BM stromal cells supplemented with human cytokines. For #2, the $CD34^+$ fraction of the patient, 2 huBM-sc samples, 1 murine BM sample, and an in vitro expanded sample were analyzed. As shown in Figure 5A, several mutations were detected with approximately 50% VAF, including those in *XBP1*, *APC*, *RPTOR*, *FLNC*, and *MLL2*, which were detected at the start in the huBM-sc samples and in the in vitro expanded sample. In all of these cases, the inv16 and t(9;22) translocation were also detected (data not shown). In contrast, these mutations were not detected in the murine BM expanded sample, which had lost the inv16, t(9;22), and mutations indicated above. Instead, it displayed *IDH1* mutations with a VAF of 50%, which was detected only at low percentage in the diagnostics sample, and various other mutations that had remained below the detection limit in the diagnostic sample (Figure 5A), clearly indicating a change in clonal

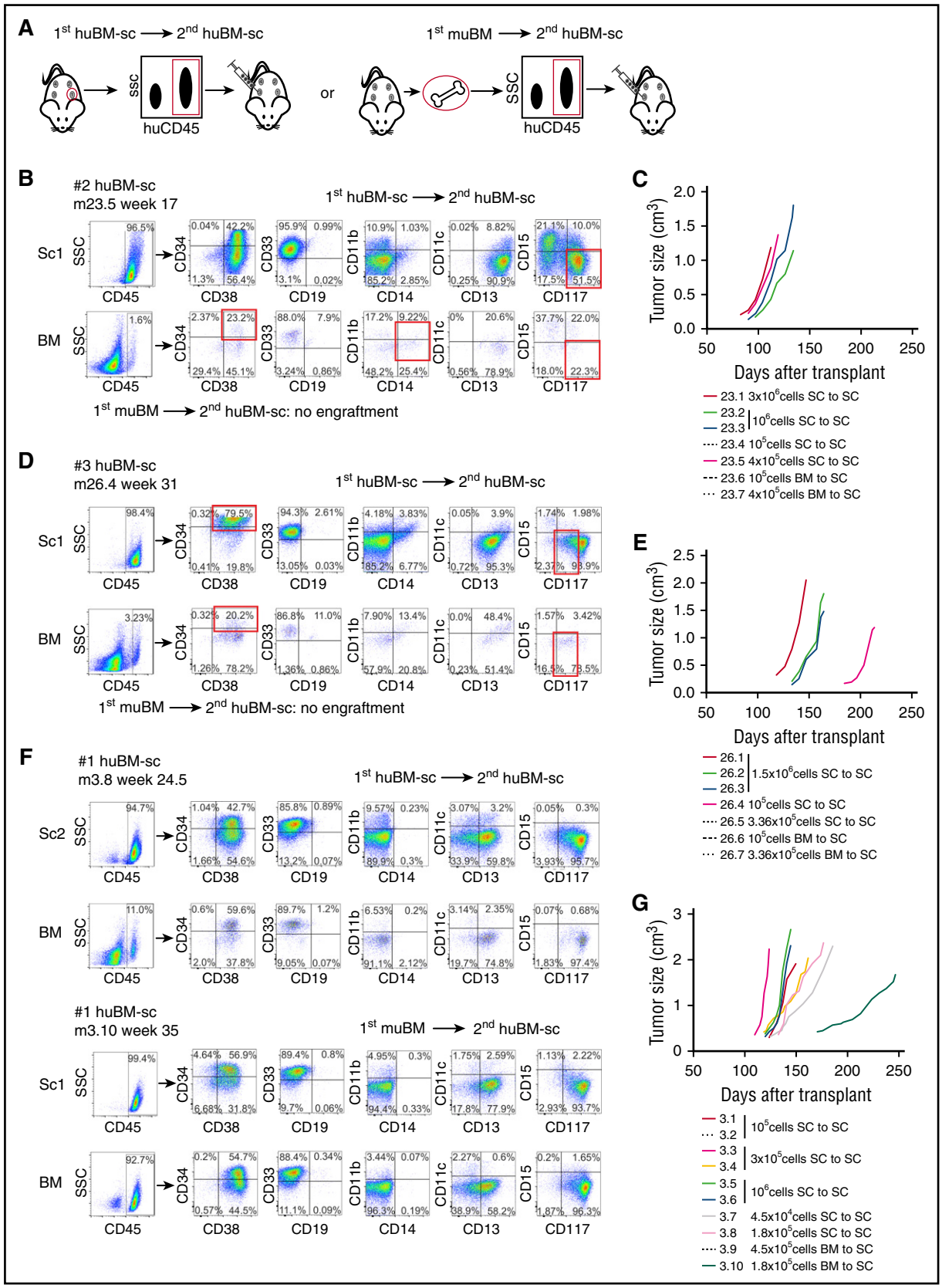

Figure 3. Assessment of the self-renewal potential of engrafting AML cells by serial transplantation of 3 AML samples. (A) Setup of secondary transplantation experiments. huCD45$^+$ cells harvested from a scaffold or from the BM of primary huBM-sc mice were injected into the scaffolds of secondary recipient NSG mice implanted with the humanized niches 6 to 8 weeks before the transplantation of leukemic cells. (B,D,F) Representative FACS analysis of secondary recipient mice of AML #2, AML #3, and AML #1, respectively. (C,E,G) In vivo tumor growth rates of the biggest tumor scaffold in secondary transplanted mice from AML #2, AML #3, and AML #1, respectively. Each colored line represents 1 mouse, and the cell dosage and source are depicted in the corresponding legend. Tumor size (cm^3) was used as the end point of the experimental period. SC, human scaffold.

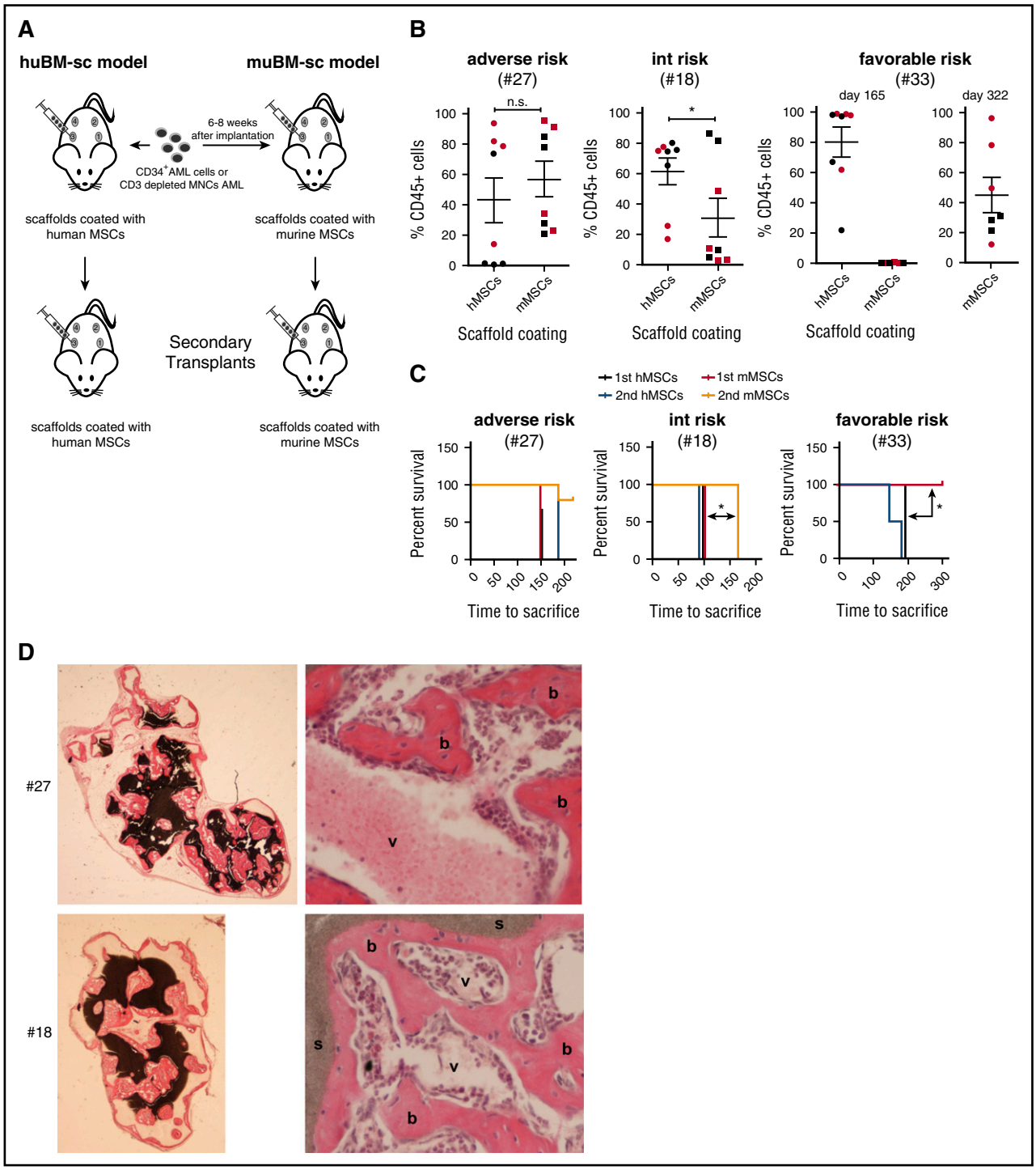

Figure 4. Assessment of the self-renewal potential of engrafting AML cells in scaffolds coated with human versus musine MSCs by serial transplantation of 3 AML samples. (A) Schematic representation of the generation of mouse models with scaffolds coated with huBM-sc vs muBM-sc. (B) Plots showing percentage of engraftment of donor human $CD45^+$ cells in the scaffolds in huBM-sc vs muBM-sc models, using patient samples with adverse, intermediate, and favorable risk. Engraftment values from 8 scaffolds in 2 mice (mouse 1 indicated with red symbols and mouse 2 indicated with black symbols) for each AML sample are expressed as mean ± SEM. (C) For secondary transplantations, leukemic cells harvested from the scaffold of a primary huBM-sc or muBM-sc mouse were injected into the scaffolds of secondary recipient huBM-sc or muBM-sc mice. Kaplan-Meier plots are shown. Significantly better secondary engraftment for the intermediate-risk sample #18 was shown in the huBM-sc model, whereas significantly better engraftment for the favorable-risk sample (#33) was already observed in the primary transplantations. (D) Ceramic scaffold implants coated with murine MSCs generate an ectopic hematopoietic niche. H&E stains of different murine implants before inoculation with AML cells. As shown the scaffolds are covered by murine bone (b) with vascularization (v), resulting in the support of the murine hematopoiesis in $Rag2^{-/-}\gamma c^{-/-}$ mice. *$P < .05$. n.s., not significant.

composition in the absence of a humanized microenviroment. For AML #1, this clonal drift was not seen, although a small clone or clones appeared with mutations in *BCOR*, *KDM6A*, *PTPN11*, and *APC* in the murine BM that was not detected at diagnosis or in the huBM-sc samples, whereas at day 43 in the in vitro expanded cells, different clones appeared with mutations in *HDAC7*, *IKZF1*, *MLL*, and *XBP1* (Figure 5B). In sample #3, the main clones with approximately 50% VAF in *NRAS*, *MSH6*, and *DNMT3A* were present at diagnosis and in

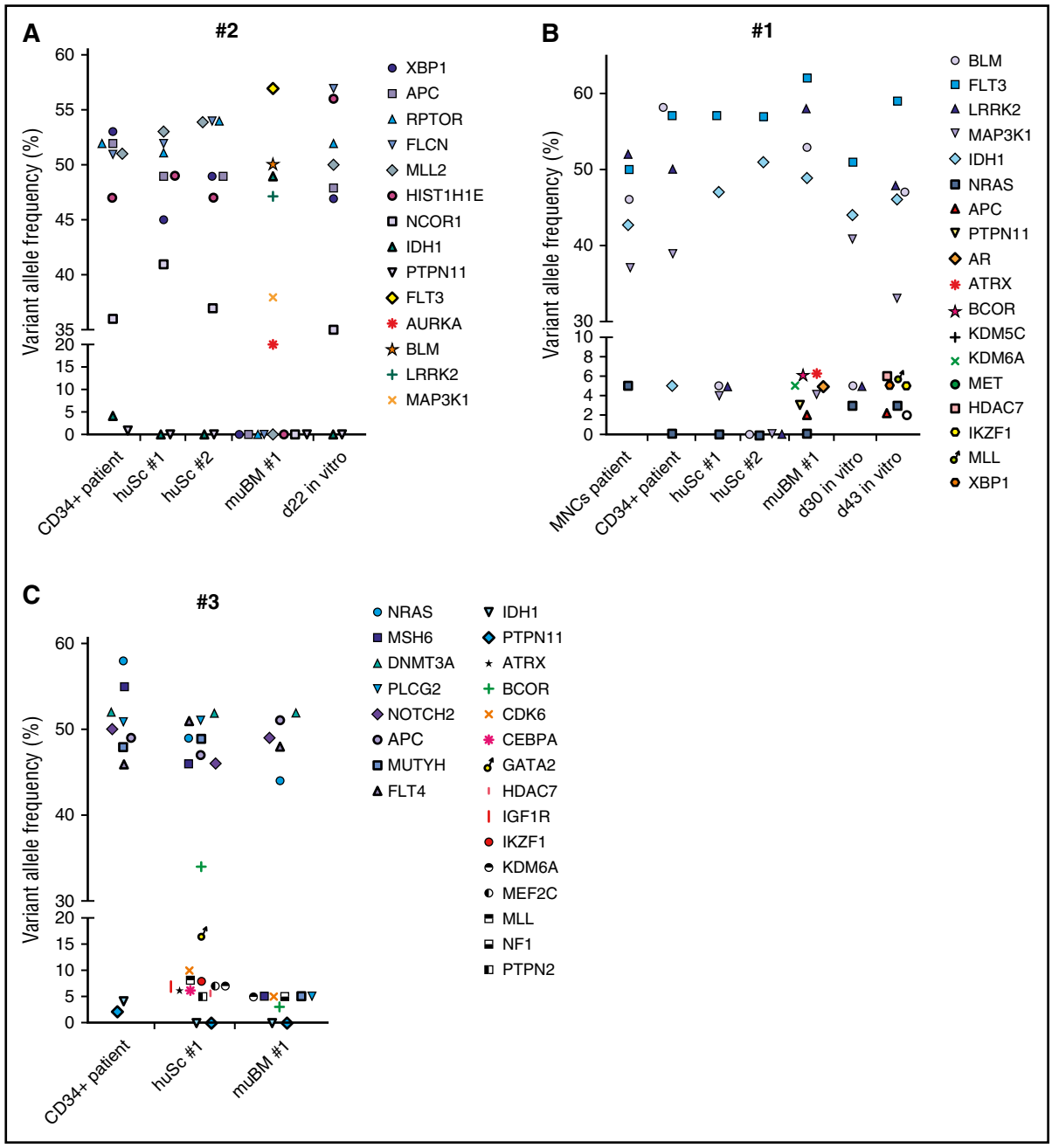

Figure 5. In vivo and in vitro maintenance of the genetic heterogeneity of the original AML patient samples. Exome sequencing to determine variant allele frequency in the leukemic populations for 3 representative AML samples: A, #2; B, #1; and C, #3. Vertical axis shows the percentage of variant reads per allele, corresponding to different somatic mutations indicated in the key. Several samples from the same AML are depicted on the horizontal axis. All samples were sorted for huCD45 expression before sequencing. VAF of ~50% indicates clonal mutations with most likely heterozygous configuration. VAF of ~100% indicates clonal mutations with homozygous configuration, whereas frequencies lower than 50% show the presence of subclonal mutations.

the huBM-sc as well as the murine BM samples. The diagnosis sample also contained mutations in *MUTYH* and *PLCG2* with a VAF of approximately 50% that was also seen in the huBM-sc sample but only at a very low VAF in the murine BM sample, suggesting that this was an independent clone that did not grow out efficiently in the murine niche. Finally, new small clones appeared with low VAF in both the huBM-sc and murine BM samples that were not detected in the diagnostic sample (Figure 5C). Together, these data clearly indicate that clonal heterogeneity and clonal drift are important parameters to evaluate in in vitro and in vivo models, and that a humanized niche might be better suited for maintaining the clonal heterogeneity observed at diagnosis.

Human MSCs are better at supporting long-term expansion of human AML compared with murine BM stroma

In vitro experiments were performed by using human MSCs, murine MS5 BM stromal cells, or liquid culture without stroma using #2 and #1 as representative examples. In all cases, $CD34^+$-sorted AML cells were grown with or without a cocktail of human cytokines, IL-3, G-CSF, and thrombopoietin, as previously described.[21-23] No long-term cultures could be established without stroma, although some expansion was observed for #2 in liquid culture conditions with cytokines, but within 20 days, cells differentiated and stopped expanding (supplemental

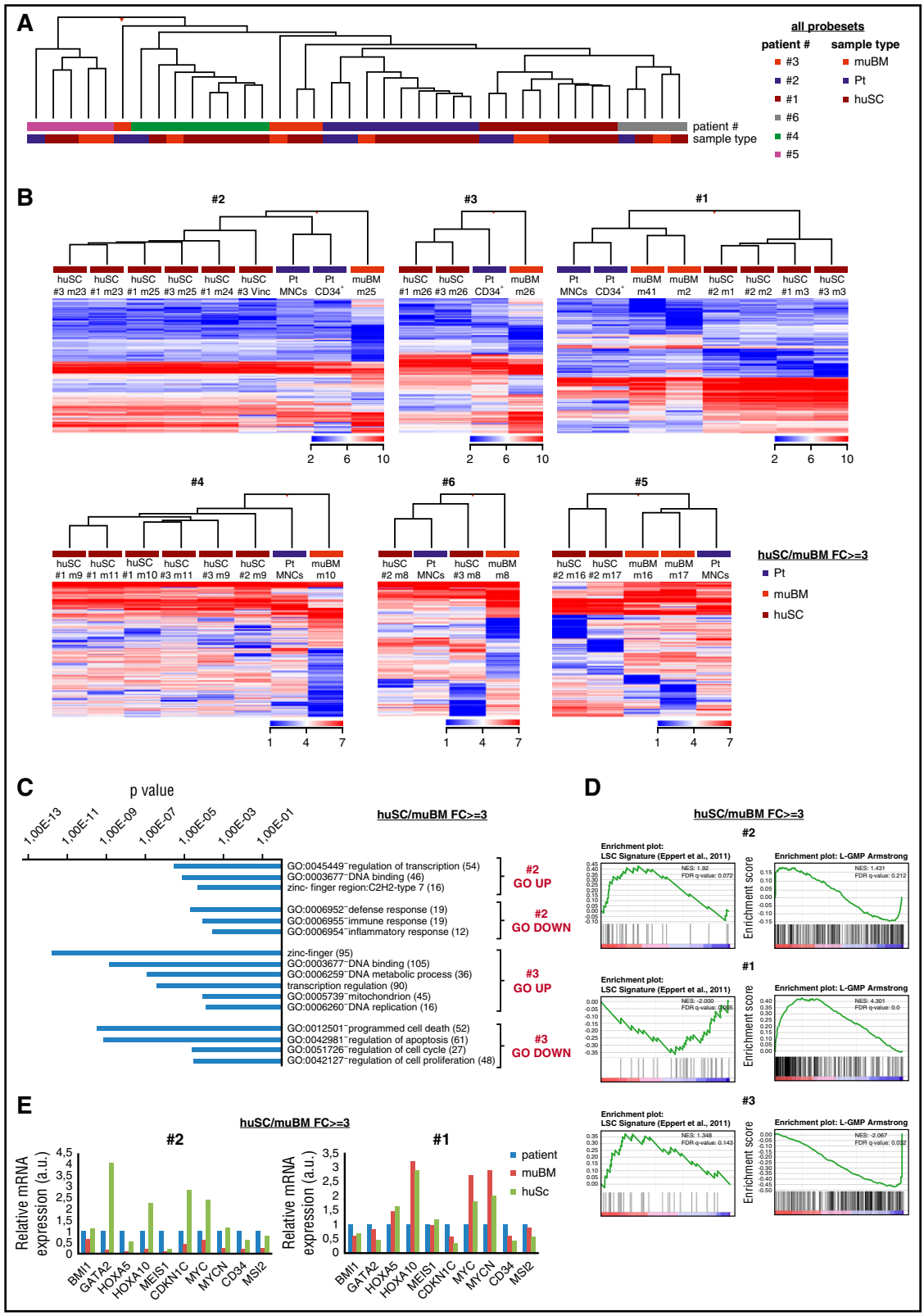

Figure 6. Gene expression profiling of AML cells derived from patients and engrafted in the humanized or murine hematopoietic niche of huBM-sc mice. (A) Unsupervised hierarchical cluster analysis (Pearson uncentered absolute distance, average linkage) on gene expression profiles of murine BM- or human scaffold (SC) –engrafted huCD45$^+$ cells or patient-derived (MNCs or CD34$^+$) leukemic cells from 6 different AMLs. (B) Supervised cluster with Euclidean distance and ward linkage analyses per AML using genes that were differentially expressed between huBM-sc– and murine BM–retrieved cells (fold change [FC] ≥3). (C) Gene ontology (GO) analyses on genes that were differentially expressed between huBM-sc– and murine BM–retrieved cells (FC ≥3). (D) Gene set enrichment analyses on genes that were differentially expressed between cells retrieved from huBM-sc and murine BM (FC ≥3). (E) Expression of individual stem cell–related genes in the diagnostic patient sample and in cells retrieved from huBM-sc and murine BM. LSC, leukemic stem cell; Pt, patient.

Figure 5A). Human MSCs clearly were superior in supporting long-term expansion of both AML samples even in the absence of additional cytokines (supplemental Figure 5A). The addition of cytokines did further enhance expansion in murine MS5 and human MSC co-cultures, but the immature $CD117^+$ phenotype was clearly better preserved in the absence of cytokines, in particular for AML #2 and to a lesser degree for AML #1 (supplemental Figure 5B-C).

Stemness transcriptome signatures are better preserved in a humanized niche

Transcriptome studies were performed on diagnostic samples as well as on huBM-sc– and murine BM–derived samples from leukemic mice for 6 patient samples (supplemental Table 3). Unsupervised hierarchical cluster analysis revealed that each patient displayed a unique transcriptome signature regardless of where cells were retrieved from (huBM-sc, murine BM, or diagnostic sample) (Figure 6A). Supervised clustering within individual patient samples revealed that diagnostic samples clustered most closely together with the huBM-sc samples for AML cases #2, #3, #4, and #6 (Figure 6B). This was not the case for AML #1 (we had already observed that this sample was less dependent on a human environment for its self-renewal and stemness properties) or for B-ALL sample #5 (Figure 6B). Gene ontology analyses revealed that specific gene sets were differently regulated in the human and murine niches, including processes such as transcription regulation, immune response, inflammatory response, mitochondria, and apoptosis regulation (Figure 6C). In line with our secondary transplantation studies, gene set enrichment analyses revealed significant enrichment for leukemic stem cell signatures for #2 and #3 when grown in the humanized scaffold compared with the murine BM, whereas this was not observed for sample #1 (Figure 6D). Instead, a significant enrichment for leukemic-granulocytic-monocytic progenitor cell signatures was observed (Figure 6D). Examples of gene expression of individual genes are shown in Figure 6E, indicating that expression of stem cell–related genes such as *BMI1*, *HOXA5*, *HOXA9*, *CD34*, *CDKN1C*, and *GATA2* was better preserved in the human niche compared with the murine niche for AML #2, whereas this was much less explicit for AML #1.

Discussion

Hematopoietic stem cells do not simply live alone, and the same holds true for leukemic stem cells. They are surrounded by a variety of other cell types that together constitute the stem cell niche in the BM.[24-28] To begin to understand mechanisms that regulate self-renewal, differentiation, and transformation of human hematopoietic stem cells, both intrinsic mechanisms and extrinsic mechanisms that involve cues from the environment need to be taken into account.[29,30] Even though the currently available immune-deficient NSG xenograft mouse models are considered the gold standard for evaluating engraftment of human hematologic malignancies, these models have serious drawbacks because only a limited percentage of primary AML patient samples can engraft, and these models are strongly lymphoid biased.[1-8] Clearly, a human BM microenvironment that would provide a suitable home for normal and leukemic stem cells is lacking in these animals. To capture and maintain stem cell self-renewal programs and clonal heterogeneity as is observed in patients, a human niche seems to be essential.

By making use of scaffolds coated with human MSCs to create a humanized environment in mice, we have established human xenograft mouse leukemia models that can serve as a resource for studying leukemic stem cells and for evaluating novel therapeutic approaches. We find that providing a humanized environment helps accomplish several things. First, 29 (74%) of 39 leukemia cases could efficiently engraft in the huBM-sc model, covering all important genetic subtypes and risk groups; all favorable-risk inv16 patient samples could also engraft, which are notoriously difficult to engraft in NSG mice. Second, stem cell self-renewal is better preserved in essentially all investigated cases in the huBM-sc compared with the mouse BM niche as determined by serial transplantation assays. Third, clonal heterogeneity as observed in the original patient is much better preserved in the huBM-sc compared with the mouse BM, at least in one case, and fourth, stem cell self-renewal signatures are better preserved in the huBM-sc in the majority of cases. Even when cells were injected intravenously into mice carrying human scaffolds, better engraftment was observed in all 5 cases that were studied, whereas in 3 of 5 cases, no or hardly any engraftment was observed at all in the mouse BM compartment. When scaffolds were coated with mouse MSCs instead of human MSCs, a favorable-risk sample failed to engraft, and an intermediate-risk sample engrafted less efficiently in primary mice, and not at all in secondary mice. During the course of our studies, Reinisch et al[31] also described that ossicles generated by injecting human MSCs with matrigel in xenograft mice could generate a humanized niche in which leukemia patient samples could engraft more efficiently, including favorable-risk PML-RARa samples, which are notoriously difficult to engraft in normal NSG mice. These data are nicely in line with ours and provide independent confirmation of the robustness of these humanized niche xenograft mouse models, but we also provide evidence that stem cell self-renewal is better preserved in a humanized niche as determined by transcriptome studies and serial transplantations.

Obviously, heterogeneity exists among leukemia patients, and we find that some patient samples are more dependent on the presence of a human niche than others. As examples, we extensively studied 2 cases: AML #2, which strongly depended on a humanized environment, and AML #1, for which this was much less the case. Consistently, AML #2 could not engraft when intravenously injected into mice without human scaffolds. The original patient phenotype identified by flow and transcriptome signatures defined by genome-wide transcriptome studies were better maintained in the human scaffolds, self-renewal properties were better preserved in the human scaffolds, and finally, the dominant BCR-ABL/inv16 clone that was present in the original patient sample also grew out in humanized scaffolds. In the mouse BM, this clone was absent, and instead, a minor clone carrying an IDH1 mutation was expanded. Similar observations were published by others,[32] showing that upon transplantation of AML samples in NSG or even NSG-SGM3 mice, clonal drift can occur, stressing the need for careful genomic analysis of engrafted clones. At the other end of the spectrum, AML #1 could also engraft when injected intravenously into mice without human scaffolds; the original patient phenotype defined by flow and transcriptome signatures was more comparable between human and murine niches, and secondary engraftment could be achieved with murine BM–harvested cells as well, albeit with lower frequencies compared with cells retrieved from human BM scaffolds.

Overall, our data indicate that the humanized scaffold models will serve as an excellent resource for future studies aimed at exploring novel therapeutic approaches. Experiments were carried out independently in 2 institutes using 2 different mouse strains (NSG and $RAG2^{-/-}\gamma c^{-/-}$), showing the robustness of the model. Clinical trials often fail when they evaluate drugs that seemed to be successful in both in vitro and in vivo studies[33,34]; in part, this might be related to the models used when a humanized environment was not included. Our current model also allows for efficient evaluation of drug efficacy, as already documented for multiple myeloma[18] and MLL-AF9 models,[35] indicating that the human leukemia xenograft mouse models that we

have established here will serve as an excellent resource for future studies aimed at exploring novel therapeutic approaches.

Acknowledgments

We acknowledge G.J. Schuurhuis for providing clinical data for a subset of acute myeloid leukemia specimens and thank G. Vanasse (Novartis, Boston, MA) for help with exome sequencing.

This work was supported by Grant No. ERC-2011-StG 281474 from the European Research Council (J.J.S.) and by Grant No. VU2011-5127 from the Dutch Cancer Foundation (R.W.J.G.).

Authorship

Contribution: J.J.S. and R.W.J.G. provided conceptual design of experiments; A.A., J.J., and J.J.S. performed mouse studies at the University Medical Center Groningen (Groningen, The Netherlands); W.A.N., R.d.J.-K., L.L.-A., A.C.M.M., and R.W.J.G. performed mouse studies at the Vrije Universiteit Medical Center (Amsterdam, The Netherlands); J.F.v.V. and A.C.B. analyzed fluorescence-activated cell sorting data; A.Z.B.-V. and J.J.S performed and analyzed transcriptome studies; H.Y. and J.D.d.B. provided scaffold material; A.A., B.d.B., W.A.N., G.J.O., E.V., A.C.M.M., R.W.J.G., and J.J.S. analyzed data; and A.A., R.W.J.G., and J.J.S. wrote the manuscript.

Conflict-of-interest disclosure: The authors declare no competing financial interests.

ORCID profiles: A.A., 0000-0003-1497-3586.

Correspondence: Jan Jacob Schuringa, Department of Experimental Hematology, Cancer Research Center Groningen, University Medical Center Groningen, University of Groningen, Hanzeplein 1, DA13, 9700RB, Groningen, The Netherlands; e-mail: j.j.schuringa@umcg.nl; and Richard W. J. Groen, Department of Hematology, Vrije Universiteit Medical Center, De Boelelaan 1117, PK2 BR012, 1081HV, Amsterdam, The Netherlands; e-mail: r.groen@vumc.nl.

References

1. Barabé F, Kennedy JA, Hope KJ, Dick JE. Modeling the initiation and progression of human acute leukemia in mice. *Science*. 2007;316(5824):600-604.
2. Horton SJ, Jaques J, Woolthuis C, et al. MLL-AF9-mediated immortalization of human hematopoietic cells along different lineages changes during ontogeny. *Leukemia*. 2013;27(5):1116-1126.
3. Rizo A, Horton SJ, Olthof S, et al. BMI1 collaborates with BCR-ABL in leukemic transformation of human CD34+ cells. *Blood*. 2010;116(22):4621-4630.
4. Wei J, Wunderlich M, Fox C, et al. Microenvironment determines lineage fate in a human model of MLL-AF9 leukemia. *Cancer Cell*. 2008;13(6):483-495.
5. Townsend EC, Murakami MA, Christodoulou A, et al. The Public Repository of Xenografts Enables Discovery and Randomized Phase II-like Trials in Mice. *Cancer Cell*. 2016;29(4):574-586.
6. Vargaftig J, Taussig DC, Griessinger E, et al. Frequency of leukemic initiating cells does not depend on the xenotransplantation model used. *Leukemia*. 2012;26(4):858-860.
7. Sanchez PV, Perry RL, Sarry JE, et al. A robust xenotransplantation model for acute myeloid leukemia. *Leukemia*. 2009;23(11):2109-2117.
8. Wunderlich M, Chou FS, Link KA, et al. AML xenograft efficiency is significantly improved in NOD/SCID-IL2RG mice constitutively expressing human SCF, GM-CSF and IL-3. *Leukemia*. 2010;24(10):1785-1788.
9. Nicolini FE, Cashman JD, Hogge DE, Humphries RK, Eaves CJ. NOD/SCID mice engineered to express human IL-3, GM-CSF and Steel factor constitutively mobilize engrafted human progenitors and compromise human stem cell regeneration. *Leukemia*. 2004;18(2):341-347.
10. Feuring-Buske M, Gerhard B, Cashman J, Humphries RK, Eaves CJ, Hogge DE. Improved engraftment of human acute myeloid leukemia progenitor cells in beta 2-microglobulin-deficient NOD/SCID mice and in NOD/SCID mice transgenic for human growth factors. *Leukemia*. 2003;17(4):760-763.
11. Goyama S, Wunderlich M, Mulloy JC. Xenograft models for normal and malignant stem cells. *Blood*. 2015;125(17):2630-2640.
12. Rongvaux A, Willinger T, Martinek J, et al. Development and function of human innate immune cells in a humanized mouse model. *Nat Biotechnol*. 2014;32(4):364-372.
13. Rongvaux A, Willinger T, Takizawa H, et al. Human thrombopoietin knockin mice efficiently support human hematopoiesis in vivo. *Proc Natl Acad Sci USA*. 2011;108(6):2378-2383.
14. Strowig T, Rongvaux A, Rathinam C, et al. Transgenic expression of human signal regulatory protein alpha in Rag2-/-gamma(c)-/- mice improves engraftment of human hematopoietic cells in humanized mice. *Proc Natl Acad Sci USA*. 2011;108(32):13218-13223.
15. Willinger T, Rongvaux A, Takizawa H, et al. Human IL-3/GM-CSF knock-in mice support human alveolar macrophage development and human immune responses in the lung. *Proc Natl Acad Sci USA*. 2011;108(6):2390-2395.
16. Willinger T, Rongvaux A, Strowig T, Manz MG, Flavell RA. Improving human hemato-lymphoid-system mice by cytokine knock-in gene replacement. *Trends Immunol*. 2011;32(7):321-327.
17. Theocharides AP, Rongvaux A, Fritsch K, Flavell RA, Manz MG. Humanized hemato-lymphoid system mice. *Haematologica*. 2016;101(1):5-19.
18. Groen RW, Noort WA, Raymakers RA, et al. Reconstructing the human hematopoietic niche in immunodeficient mice: opportunities for studying primary multiple myeloma. *Blood*. 2012;120(3):e9-e16.
19. Gutierrez A, Pan L, Groen RW, et al. Phenothiazines induce PP2A-mediated apoptosis in T cell acute lymphoblastic leukemia. *J Clin Invest*. 2014;124(2):644-655.
20. Schuringa JJ, Chung KY, Morrone G, Moore MA. Constitutive activation of STAT5A promotes human hematopoietic stem cell self-renewal and erythroid differentiation. *J Exp Med*. 2004;200(5):623-635.
21. Schuringa JJ, Schepers H. Ex vivo assays to study self-renewal and long-term expansion of genetically modified primary human acute myeloid leukemia stem cells. *Methods Mol Biol*. 2009;538:287-300.
22. Sontakke P, Carretta M, Capala M, Schepers H, Schuringa JJ. Ex vivo assays to study self-renewal, long-term expansion, and leukemic transformation of genetically modified human hematopoietic and patient-derived leukemic stem cells. *Methods Mol Biol*. 2014;1185:195-210.
23. van Gosliga D, Schepers H, Rizo A, van der Kolk D, Vellenga E, Schuringa JJ. Establishing long-term cultures with self-renewing acute myeloid leukemia stem/progenitor cells. *Exp Hematol*. 2007;35(10):1538-1549.
24. Calvi LM, Link DC. The hematopoietic stem cell niche in homeostasis and disease. *Blood*. 2015;126(22):2443-2451.
25. Calvi LM, Adams GB, Weibrecht KW, et al. Osteoblastic cells regulate the haematopoietic stem cell niche. *Nature*. 2003;425(6960):841-846.
26. Zhang J, Niu C, Ye L, et al. Identification of the haematopoietic stem cell niche and control of the niche size. *Nature*. 2003;425(6960):836-841.
27. Méndez-Ferrer S, Michurina TV, Ferraro F, et al. Mesenchymal and haematopoietic stem cells form a unique bone marrow niche. *Nature*. 2010;466(7308):829-834.
28. Schepers K, Campbell TB, Passegué E. Normal and leukemic stem cell niches: insights and therapeutic opportunities. *Cell Stem Cell*. 2015;16(3):254-267.
29. Enver T, Pera M, Peterson C, Andrews PW. Stem cell states, fates, and the rules of attraction. *Cell Stem Cell*. 2009;4(5):387-397.
30. Eaves CJ. Hematopoietic stem cells: concepts, definitions, and the new reality. *Blood*. 2015;125(17):2605-2613.
31. Reinisch A, Thomas D, Corces MR, et al. A humanized bone marrow ossicle xenotransplantation model enables improved engraftment of healthy and leukemic human hematopoietic cells. *Nat Med*. 2016;22(7):812-821.
32. Klco JM, Spencer DH, Miller CA, et al. Functional heterogeneity of genetically defined subclones in acute myeloid leukemia. *Cancer Cell*. 2014;25(3):379-392.
33. Alizadeh AA, Aranda V, Bardelli A, et al. Toward understanding and exploiting tumor heterogeneity. *Nat Med*. 2015;21(8):846-853.
34. Gould SE, Junttila MR, de Sauvage FJ. Translational value of mouse models in oncology drug development. *Nat Med*. 2015;21(5):431-439.
35. Sontakke P, Carretta M, Jaques J, et al. Modeling BCR-ABL and MLL-AF9 leukemia in a human bone marrow-like scaffold-based xenograft model. *Leukemia*. 2016;30(10):2064-2073.